Can Weak Chirality Induce Strong Coupling between Resonant States?

Yang Chen,[1,2] Weijin Chen,[2] Xianghong Kong,[2] Dong Wu,[1] Jiaru Chu,[1] and Cheng-Wei Qiu[2,*]
[1]Chinese Academy of Sciences Key Laboratory of Mechanical Behavior and Design of Materials, Department of Precision Machinery and Precision Instrumentation, University of Science and Technology of China, 230027 Hefei, China
[2]Department of Electrical and Computer Engineering, National University of Singapore, 117583 Singapore, Singapore

(Received 3 November 2021; accepted 21 March 2022; published 6 April 2022)

Strong coupling between resonant states is usually achieved by modulating intrinsic parameters of optical systems, e.g., the refractive index of constituent materials or structural geometries. Externally introduced chiral enantiomers may couple resonances, but the extremely weak chirality of natural enantiomers largely prevents the system from reaching strong coupling regimes. Whether weak chirality could induce strong coupling between resonant states remains an open question. Here, we realize strong coupling between quasibound states in the continuum of a high-Q metasurface, assisted with externally introduced enantiomers of weak chirality. We establish a chirality-involved Hamiltonian to quantitatively describe the correlation between the coupling strength and the chirality of such systems, which provides an insightful recipe for enhancing the coupling of resonant states further in the presence of quite weak chirality. Consequently, high-sensitivity chiral sensing is demonstrated, in which the circular dichroism signal is enhanced 3 orders higher than the case without strong coupling. Our findings present a distinct strategy for manipulating optical coupling between resonances, revealing opportunities in chiral sensing, topological photonics, and quantum optics.

DOI: 10.1103/PhysRevLett.128.146102

Mode coupling is a cornerstone of modern photonics, giving rise to many important phenomena, such as Fano resonance [1,2], electromagnetically induced transparency [3,4], bound states in the continuum (BIC) [5,6], and parity-time (PT) symmetry [7,8]. In most cases, optical systems are dissipative and lose their energy by radiation and/or absorption, whose eigenstates are referred to as quasinormal modes or resonant states [9–11]. The optical coupling between resonant states has found wide applications in biosensing [12], lasering [13], nonlinear optics [14], and topological photonics [15].

The most fundamental coupling system involves two resonant states in a cavity. The coupling can be classified into weak coupling if $g < \gamma 1$ or $g < \gamma 2$ and strong coupling if $g > \gamma 1$ and $g > \gamma 2$, where $\gamma 1$ and $\gamma 2$ are the decay rates of the two resonant states and g is the rate of energy exchange between the two resonances. Generally, the coupling strength g is engineered by the shapes of optical structures [16–18] or the refractive index of constituent materials [19,20], both of which lead to the intrinsic modulation of the optical system. Apart from this well-studied strategy, mode coupling can also be induced through the extrinsic introduction of chiral enantiomers [21–23], whose nonzero Pasteur parameter κ enables magnetoelectric interactions. However, the research of chirality-induced coupling has long been impeded by the extremely weak κ of natural chiral enantiomers (e.g., amino acids, proteins, and sugars), typically at the order of 10^{-5}–10^{-4} [24]. As a consequence, the achievable coupling strength is very weak, and it remains an open question: Can weak chirality induce strong coupling between resonant states?

In this work, for the first time, we have realized strong coupling between two quasibound states in the continuum (quasi-BICs) in a metasurface, assisted with externally introduced enantiomers of weak chirality. The concept of BIC has recently been introduced into photonics to describe the electromagnetic state completely decoupled from the radiating waves while lying inside the continuum spectrum of radiation modes [25–28], although this phenomenon has been discovered before [29–33]. When BIC is converted to quasi-BIC through geometric perturbations or slanted incidence, it will possess an ultrahigh yet finite Q factor. We establish a chirality-involved Hamiltonian to quantitatively evaluate the chirality-induced coupling strength between two resonant states, based on which an insightful design recipe is proposed to enhance such coupling. Large Rabi splitting and strong loss redistribution are observed in the strong coupling system. We demonstrate that the proposed coupling system can enhance the circular dichroism (CD) signal of chiral enantiomers for a record 3000 times relative to the case without the coupling.

We first consider an optical cavity without chiral enantiomers, supporting two resonant states. Their fields $\boldsymbol{E}_i$ and $\boldsymbol{H}_i$ satisfy Maxwell's equations: $\nabla \times \boldsymbol{E}_i = -i\omega_i \mu \boldsymbol{H}_i$ and $\nabla \times \boldsymbol{H}_i = i\omega_i \varepsilon \boldsymbol{E}_i$, where the subscript $i = 1, 2$ labels the two resonances and ε and μ are the permittivity and permeability. When chiral enantiomers are introduced into the cavity, the two resonances are coupled and hybridized

into two supermodes. The fields of the two supermodes, as the superposition of two original resonances, can be expressed as $\boldsymbol{E} = \sum a_j \boldsymbol{E}_j$ and $\boldsymbol{H} = \sum a_j \boldsymbol{H}_j$, where a_j is the coefficient to be determined. The supermodes satisfy Maxwell's equations: $[\nabla \times + i\omega(i\kappa/c_0)]\Sigma a_j \boldsymbol{E}_j = -i\omega\mu\Sigma a_j \boldsymbol{H}_j$ and $[\nabla \times - i\omega(i\kappa/c_0)]\Sigma a_j \boldsymbol{H}_j = i\omega\varepsilon\Sigma a_j \boldsymbol{E}_j$. By combining all these equations, the general eigenvalue equation in matrix form is given as

$$Ax = \omega B x, \tag{1}$$

where $A = \begin{bmatrix} -\omega_1 p_{11} & -\omega_2 p_{12} \\ -\omega_1 p_{21} & -\omega_2 p_{22} \end{bmatrix}$, $B = \begin{bmatrix} (i\kappa/c_0)k_{11} - p_{11} & (i\kappa/c_0)k_{12} - p_{12} \\ (i\kappa/c_0)k_{21} - p_{21} & (i\kappa/c_0)k_{22} - p_{22} \end{bmatrix}$, $k_{ij} = \iiint_V dV(E_i \cdot H_j + H_i \cdot E_j)$, $p_{ij} = \iiint_V dV(E_i \cdot \varepsilon E_j - H_i \cdot \mu H_j)$, and $x = \binom{a_1}{a_2}$. The physical meaning of p_{ij} and k_{ij} can be found in Supplemental Material [34]. V is the mode volume to be integrated. According to Eq. (1), two eigenvalues $\omega_\pm$ and their corresponding eigenvectors x can be acquired for the two supermodes. The Hamiltonian of the coupled system is derived as

$$\mathscr{H} = B^{-1}A. \tag{2}$$

Here, without the loss of generality, three assumptions are employed to guarantee that the coupling of resonant states is solely originated from the externally introduced chiral enantiomers. (i) The two uncoupled resonant states are orthogonal, and, thus, the terms p_{12} and p_{21} are much smaller than p_{11} and p_{22}. (ii) The structure of the cavity itself is nonchiral, and, thus, the intramode coupling terms k_{11} and k_{22} are much smaller than the intermode coupling terms k_{12} and k_{21}. (iii) Since the amplitude of κ is much smaller than ε and μ for natural enantiomers [24], the inequality $(i\kappa/c_0)^2 k_{12}k_{21} \ll p_{11}p_{22}$ is satisfied (Supplemental Material [34]). Then, the Hamiltonian $\mathscr{H}$ is simplified as

$$\mathscr{H} = \begin{pmatrix} \omega_1 & \frac{i\kappa}{c_0}\frac{k_{12}\omega_2}{p_{11}} \\ \frac{i\kappa}{c_0}\frac{k_{21}\omega_1}{p_{22}} & \omega_2 \end{pmatrix}, \tag{3}$$

For the first time, we have derived closed-form expressions to analytically evaluate the chirality-induced coupling strength g between two resonant states in a cavity. Although the derived Hamiltonian $\mathscr{H}$ basically follows the general form of coupled-mode theory [38,39], the off-orthogonal terms, responsible for chirality-induced coupling, have been specified, which suggests a design recipe for achieving chirality-induced strong coupling. The eigenvalues can be solved as

$$\omega_\pm = \frac{1}{2}\left(\omega_1 + \omega_2 \pm \frac{\sqrt{p_{11}p_{22}(\omega_1 - \omega_2)^2 + 4(\frac{i\kappa}{c_0})^2 k_{12}k_{21}\omega_1\omega_2}}{\sqrt{p_{11}}\sqrt{p_{22}}}\right), \tag{4}$$

At zero detuning $\omega_1 = \omega_2$, Eq. (4) is reduced to

$$\omega_\pm = \frac{1}{2}(\omega_1 + \omega_2) \pm \frac{\kappa}{c_0}\sqrt{\frac{-k_{12}k_{21}\omega_1\omega_2}{p_{11}p_{22}}}, \tag{5}$$

Suppose κ is fixed and small; the fields of the two resonances should obey electromagnetic duality. Then, k_{12} and k_{21}, calculated as the integration of field overlap between the two resonances, are maximized, while p_{11} and p_{22} are constants if the two resonant states are under proper normalization (Supplemental Material [34]). Another key requirement is that the two resonant states should possess high Q factors, implying small decay rates.

Next, we will demonstrate chirality-induced strong coupling between two quasi-BICs. The paradigmatic system is a dielectric metasurface composed of periodic holes inside a slab ($n = 2.4$) on a substrate ($n = 1.45$) as shown in Fig. 1(a). The solution on top of the metasurface has properties $\varepsilon_{\mathbf{r}} = 2.1 + 2i \times 10^{-4}$ and $\mu_{\mathbf{r}} = 1 + 2i \times 10^{-5}$. Because of the existence of perturbative cuts Δ, the metasurface supports a series of quasi-BICs with high Q factors at the Γ point of the Brillouin zone (Supplemental Material [34]). These quasi-BICs belong to TE- or TM-like modes (shortened as TE and TM mode, respectively, for brevity), according to the symmetry of electromagnetic fields upon mirror transformations. Specifically, we will investigate the coupling between TE_4 and TM_1 quasi-BICs, because they are well isolated from other Bloch modes and their fields approximately satisfy electromagnetic duality [Fig. 1(b)]. Coupling between other combinations of quasi-BICs can be found in Supplemental Material [34]. By finely tuning the slab thickness t to be 165.9 nm, the two quasi-BICs become degenerate at the Γ point as depicted in Fig. 1(b) Supplemental Material [34]). No coupling is expected for these two quasi-BICs in the absence of chiral enantiomers due to their orthogonality.

When a certain amount of chiral enantiomers are introduced into the solution, the solution will acquire a nonzero κ. Here, the general theory developed by Govorov and co-workers is utilized to model the chiral solution [40], and κ is assumed to be $(2 + 0.4i) \times 10^{-4}$ (Supplemental Material [34]), which falls within the range of common chiral materials. Induced by the chiral enantiomers, two hybridized branches are formed, namely, upper branch (UB) and lower branch (LB), exhibiting an avoided crossing behavior as depicted in Fig. 1(c). The simulation and analytical calculation match very well with other. All the

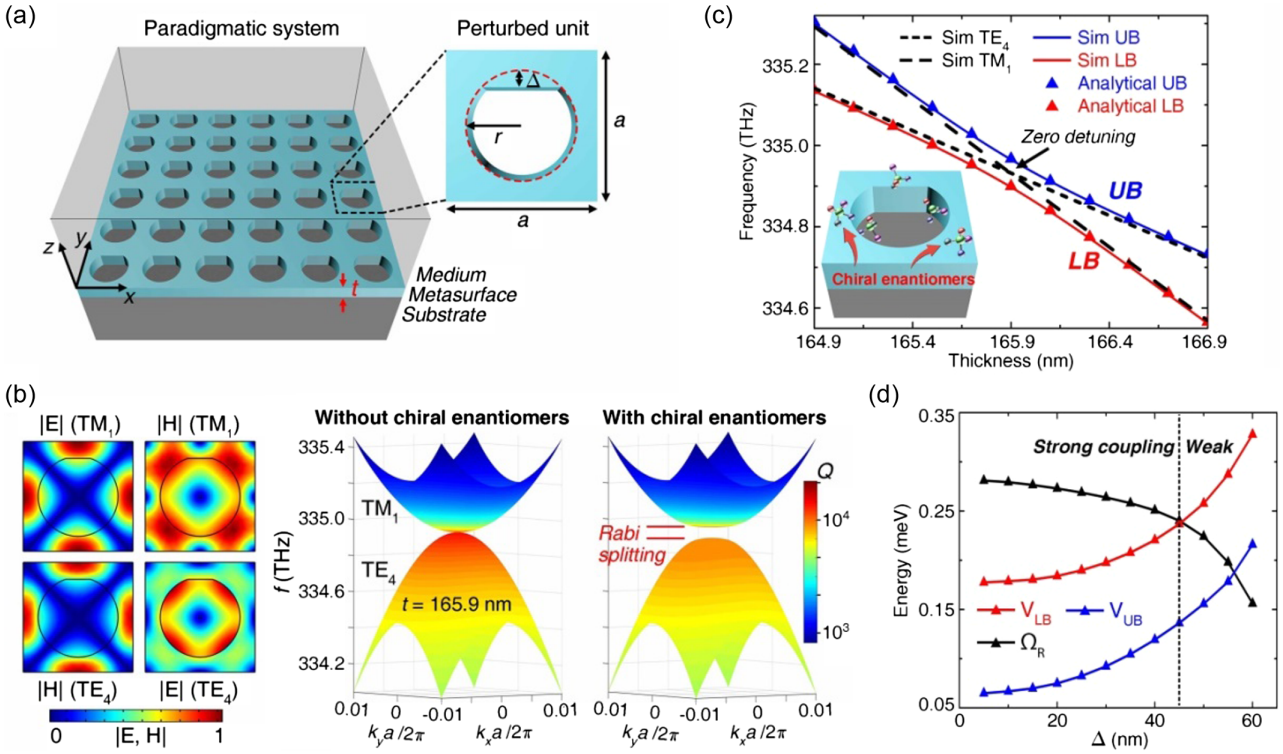

FIG. 1. Strong coupling between two quasi-BICs in a metasurface. (a) Schematic of the paradigmatic system. The geometric parameters of the metasurface are period $a = 550$ nm, radius $r = 200$ nm, perturbation size $\Delta = 10$ nm, and thickness $t = 165.9$ nm. (b) Band structures of the TM_1 and TE_4 quasi-BICs with and without chiral material. The electric and magnetic field profiles of the two uncoupled quasi-BICs are plotted on the left showing electromagnetic duality. (c) Eigenfrequencies of the UB and LB at different thicknesses t obtained by simulations and analytical calculations. The eigenfrequencies of uncoupled TM_1 and TE_4 modes form two dashed lines, intersected at the zero detuning point. (d) Rabi splitting (Ω_R) and the linewidths of the two branches (V_{UB} and V_{LB}) at different perturbation scales Δ.

simulations in this work are performed in COMSOL Multiphysics. At zero detuning $\omega_1 = \omega_2$, the Rabi splitting is calculated to be $\Omega_R = 0.279$ meV, larger than the linewidths of the two branches $V_{UB} = 0.067$ meV and $V_{LB} = 0.179$ meV, which fulfills the strict criterion of strong coupling. The large Rabi splitting is clearly observed in the momentum space [Fig. 1(b)], where the two quasi-BIC bands are detached and substantially separated.

The high Q factor of quasi-BIC is the key point for the generation of strong coupling. If the perturbation Δ is enlarged, the Q factors of both quasi-BICs will be reduced. As a result, more electromagnetic energy is radiated to the far field rather than confined in the near field, leading to a weaker coupling strength and a smaller Rabi splitting [Fig. 1(d)]. Meanwhile, the linewidths of the two branches are also increased. Beyond the critical point of $\Delta = 45$ nm, the system enters into the weak coupling regime.

The κ of chiral enantiomers can also modulate the coupling system. In Eq. (5), the expression inside the radical is fixed for a passive metasurface, and it is approximately a positive real number as proved in Supplemental Material [34]. Hence, the real part of the difference between ω_+ and ω_-, manifested as Rabi splitting, should be roughly proportional to $\mathrm{Re}(\kappa)$, while it is unchanged with $\mathrm{Im}(\kappa)$, which is confirmed in Fig. 2(a). On the other hand, the imaginary part of the difference between ω_+ and ω_-, manifested as the uneven redistribution of loss over the two branches, should primarily have a linear relationship with $\mathrm{Im}(\kappa)$, as presented in Fig. 2(b). This is another important manifestation of strong coupling, where one branch becomes more lossy than the original resonant states, and the other branch becomes less lossy [41]. Such loss redistribution by strong coupling is the basis for *Friedrich-Wintgen* BIC [41], and, therefore, our system showcases the potential to restore quasi-BIC to BIC through chirality-induced coupling. In addition, we notice that our system offers an ideal platform for investigating anti-parity-time (APT) symmetry [42,43]. If the imaginary part of κ is negligibly smaller than the real part [44], the Hamiltonian in Eq. (3) becomes a characteristic anti-PT symmetric matrix. As a result, the two resonant states have the same frequency but different linewidths before the exceptional point (EP), where the coupling strength is quite weak. Beyond the EP, their frequency is split, while their linewidths undergo a conversion from nondegeneracy to degeneracy (Fig. 2, insets).

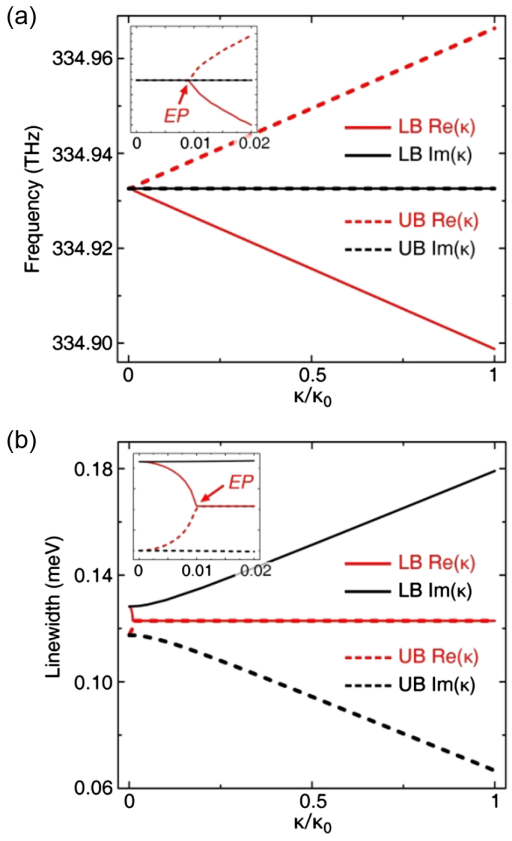

FIG. 2. The modulation of coupling system using κ. (a) Frequencies and (b) linewidths of UB and LB as functions of the real and imaginary part of κ obtained from analytical calculations. Here, the varying κ is normalized by its initial value $\kappa_0 = (2 + 0.4i) \times 10^{-4}$. The enlarged plots corresponding to the range of small κ are shown in the insets.

Within the framework of our analytical model, the hybridized modes are the superposition of original resonant states, where the coefficient a_j basically indicates the strength of hybridization. We have retrieved the coefficients $a_{\mathrm{UB},1}$ and $a_{\mathrm{UB},2}$, as well as $a_{\mathrm{LB},1}$ and $a_{\mathrm{LB},2}$ [Fig. 3(a)]. In the case of $t = 164.9$ nm, the mode coupling is weak due to the large frequency detuning. Then, the UB (LB) is mainly composed of the TE_4 (TM_1) quasi-BIC ($|a_{\mathrm{UB},1}| \approx 1$, $|a_{\mathrm{LB},2}| \approx 1$), which can also be observed from their mode profiles. When the coupling strength is maximized around zero detuning $t = 165.9$ nm, the two quasi-BICs are fully mixed with $|a_{\mathrm{UB},1}| \approx |a_{\mathrm{UB},2}|$ and $|a_{\mathrm{LB},1}| \approx |a_{\mathrm{LB},2}|$. As a result, the profiles of the two hybridized modes are almost equal combinations of the two quasi-BICs, and, thus, they exhibit very similar mode profiles. Such mode hybridization in the near field is also projected to the far field. Since the phase delays δ_{UB} and δ_{LB}, where $\delta_{\mathrm{UB}} = \arg(a_{\mathrm{UB},1}) - \arg(a_{\mathrm{UB},2})$ and $\delta_{\mathrm{LB}} = \arg(a_{\mathrm{LB},1}) - \arg(a_{\mathrm{LB},2})$, possess opposite signs as shown in Fig. 3(a), the polarization state of far-field radiation exhibits right-handed elliptical polarization for the UB and left-handed elliptical polarization for the LB [Fig. 3(b)]. Around zero detuning, the ellipticity angle of polarization approaches $\pi/4$ for the UB and $-\pi/4$ for the LB, so that their far-field radiation is approximately right-handed circularly polarized (RCP) and left-handed circularly polarized (LCP), respectively. In this way, we have constructed a nanosystem supporting chiral quasi-BICs based not on the sophisticated design of nanostructures [45–47], but on the introduction of chiral enantiomers. When the introduced chiral enantiomers change their handedness, the sign of κ is flipped, leading to the reversal of eigenpolarization for both UB and LB (Supplemental Material [34]).

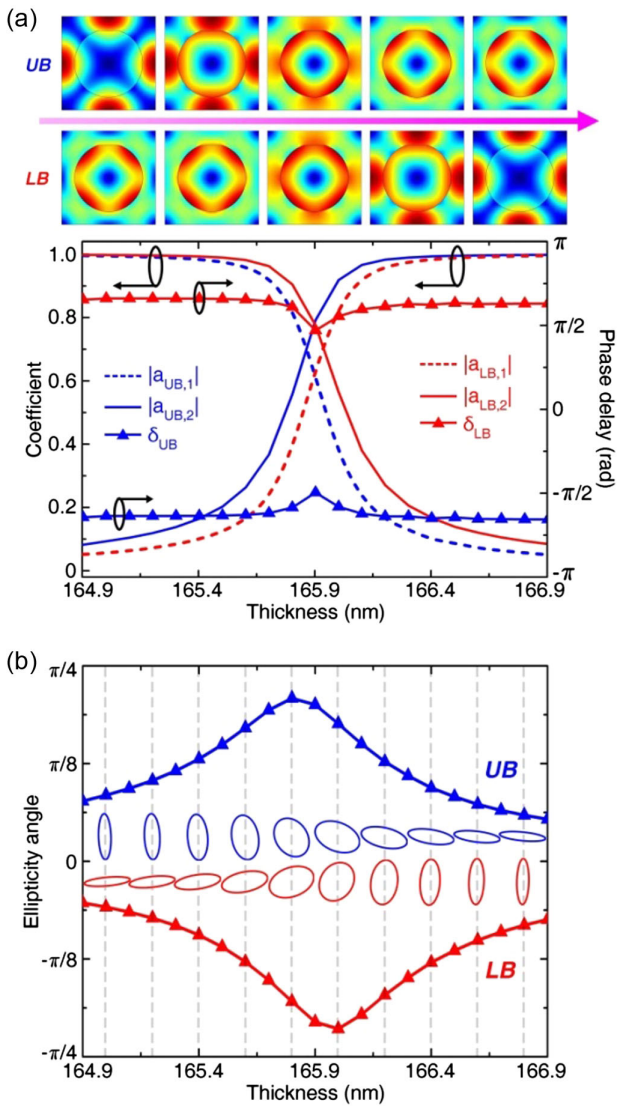

FIG. 3. Mode hybridization manifested in the near field and far field. (a) Retrieved coupling coefficients a_j for UB and LB at different thicknesses. The evolution of mode profiles for the two branches is demonstrated on the top. (b) Ellipticity angle of the far-field radiation for the two branches. The corresponding eigenpolarizations are plotted in the middle, where the blue color indicates right-handed elliptical polarization and the red color indicates left-handed elliptical polarization.

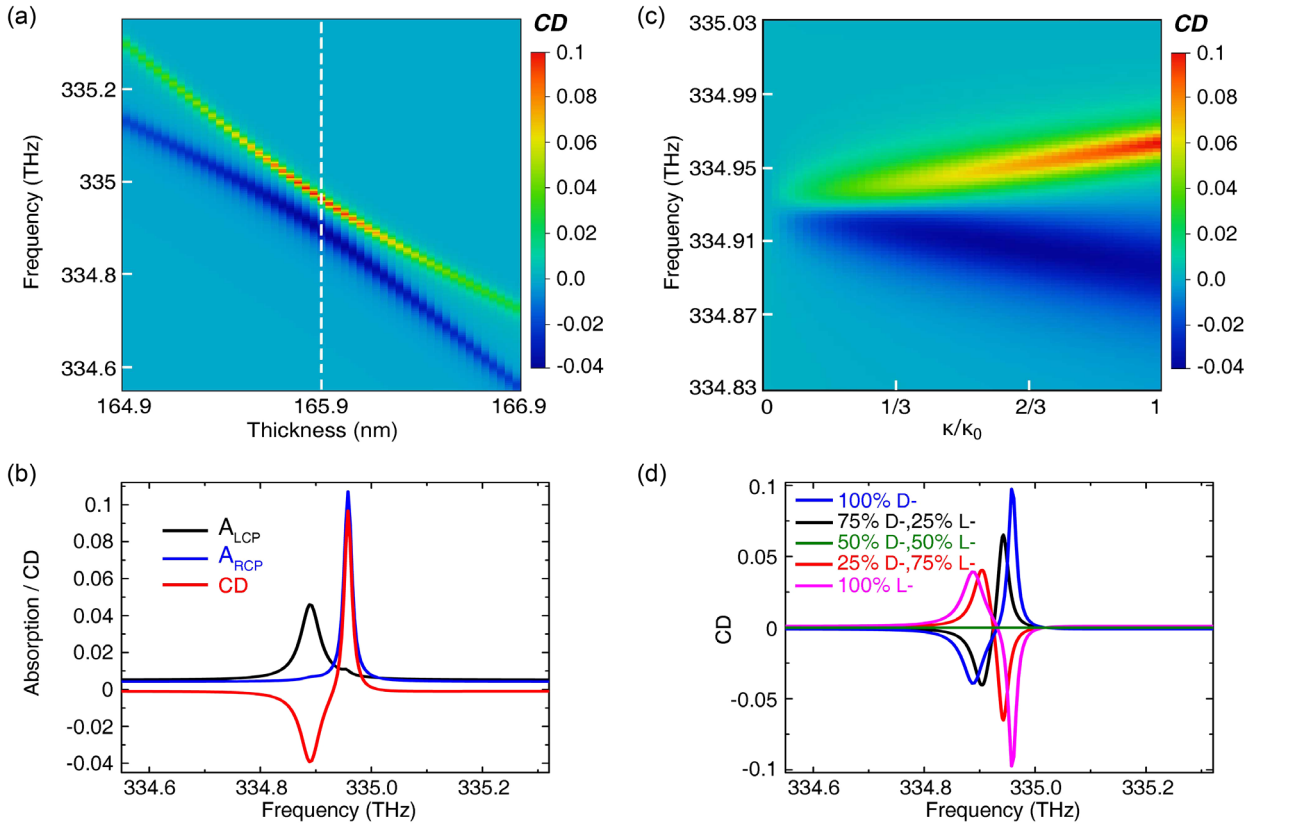

FIG. 4. Enhanced chiral sensing based on chirality-induced mode coupling. (a) Simulated CD spectra of the metasurface with different thicknesses for a fixed κ value. (b) Circular absorption and CD spectra for the case $t = 165.9$ nm, corresponding to the cut line in (a). (c) CD spectra of the metasurface with a fixed thickness ($t = 165.9$ nm) for different κ values. The varying κ is normalized by its initial value $\kappa_0 = (2 + 0.4i) \times 10^{-4}$. (d) CD spectra of the metasurface for different chiral samples.

As demonstrated above, the external introduction of chiral enantiomers is a convenient yet effective method to modulate the coupling between resonant states. On the other hand, the coupling system also provides a versatile platform for detecting chiral enantiomers. Although dielectric metasurfaces have been extensively proposed for enhancing chiral sensing [48–53], chirality-induced mode coupling has been ignored in all these works. Consequently, these works are applicable only in the weak coupling regime, where the enhancement of CD relative to the case without a metasurface is limited, smaller than 300. This problem has been overcome in our work. As shown in Fig. 4(a), when circularly polarized light is normally illuminated on the proposed system with varied metasurface thicknesses t, two pronounced CD resonance branches are observed, corresponding to the two hybridized branches in Fig. 1(c). Here, CD is defined as $\mathrm{CD} = (A_{\mathrm{RCP}} - A_{\mathrm{LCP}})/(A_{\mathrm{RCP}} + A_{\mathrm{LCP}})$, where $A_{\mathrm{RCP/LCP}}$ denotes the absorption under RCP/LCP incidence. Since the two branches possess opposite handedness for far-field radiation, their CD signals are oppositely signed. At zero detuning $t = 165.9$ nm, the maximum CD of 0.1 is achieved, which is 3000 times stronger than the case without metasurface. Such a record high CD enhancement is around 10 times larger than all the existing works, which can be attributed to the strong chirality-induced mode coupling. As observed in Fig. 4(b), the large Rabi splitting spectrally separates the two circular absorption resonances A_{RCP} and A_{LCP}, while the loss redistribution effect increases the Q factor of the UB, which, in turn, increases its absorption intensity. For this reason, the CD resonance corresponding to the LB is only -0.04. Meanwhile, with the increase of κ, the two CD resonances are linearly increased in amplitude, while their spectral gap is linearly enlarged as well [Fig. 4(c)]. Suppose the $\boldsymbol{D}$ enantiomer possesses positive κ of $(2 + 0.4i) \times 10^{-4}$ while the $\boldsymbol{L}$ enantiomer possesses negative κ of $(-2 - 0.4i) \times 10^{-4}$. We have calculated the CD spectra of chiral samples with different enantiomer excess in Fig. 4(d).

In conclusion, we have realized chirality-induced strong coupling between two quasi-BICs in a metasurface. Further, we have utilized the strong coupling system to achieve a record high 3000 times enhancement of CD signals. We believe that our findings open new horizons for engineering mode coupling by externally introducing chiral enantiomers, which offers opportunities for chiral sensing, circularly polarized lasing, and quantum optics.

We acknowledge the support from the start-up funding of University of Science and Technology of China, the CAS Pioneer Hundred Talents Program, and the National Natural Science Foundation of China (Grants No. 61731010 and No. 11874142). D. W. acknowledges the support by the National Key Scientific Instrument and Equipment Development Project (No. 61927814) and the National Natural Science Foundation of China (No. 52005475, No. 51875544, and No. 61805230). C.-W. Q. is supported by Grant No. R-261-518-004-720 from Advanced Research and Technology Innovation Centre (ARTIC).

Y. C. and W. C. contributed equally to this work.

*chengwei.qiu@nus.edu.sg

[1] B. Luk'yanchuk, N. I. Zheludev, S. A. Maier, N. J. Halas, P. Nordlander, H. Giessen, and C. T. Chong, Nat. Mater. **9**, 707 (2010).
[2] V. A. Fedotov, M. Rose, S. L. Prosvirnin, N. Papasimakis, and N. I. Zheludev, Phys. Rev. Lett. **99**, 147401 (2007).
[3] S. Zhang, D. A. Genov, Y. Wang, M. Liu, and X. Zhang, Phys. Rev. Lett. **101**, 047401 (2008).
[4] L. Verslegers, Z. Yu, Z. Ruan, P. B. Catrysse, and S. Fan, Phys. Rev. Lett. **108**, 083902 (2012).
[5] K. Koshelev, S. Lepeshov, M. Liu, A. Bogdanov, and Y. Kivshar, Phys. Rev. Lett. **121**, 193903 (2018).
[6] W. Liu, B. Wang, Y. Zhang, J. Wang, M. Zhao, F. Guan, X. Liu, L. Shi, and J. Zi, Phys. Rev. Lett. **123**, 116104 (2019).
[7] C. E. Rüter, K. G. Makris, R. El-Ganainy, D. N. Christodoulides, M. Segev, and D. Kip, Nat. Phys. **6**, 192 (2010).
[8] A. Cerjan, A. Raman, and S. Fan, Phys. Rev. Lett. **116**, 203902 (2016).
[9] P. T Leung, S. Y. Liu, and K. Young, Phys. Rev. A **49**, 3057 (1994).
[10] Q. Bai, M. Perrin, C. Sauvan, J.-P. Hugonin, and P. Lalanne, Opt. Express **21**, 27371 (2013).
[11] F. Alpeggiani, N. Parappurath, E. Verhagen, and L. Kuipers, Phys. Rev. X **7**, 021035 (2017).
[12] C. Wu, A. B. Khanikaev, R. Adato, N. Arju, A. A. Yanik, H. Altug, and G. Shvets, Nat. Mater. **11**, 69 (2012).
[13] L. Feng, Z. J. Wong, R.-M. Ma, Y. Wang, and X. Zhang, Science **346**, 972 (2014).
[14] K. Koshelev, S. Kruk, E. Melik-Gaykazyan, J. H. Choi, A. Bogdanov, H. G. Park, and Y. Kivshar, Science **367**, 288 (2020).
[15] S. Weimann, M. Kremer, Y. Plotnik, Y. Lumer, S. Nolte, K. G. Makris, M. Segev, M. C. Rechtsman, and A. Szameit, Nat. Mater. **16**, 433 (2017).
[16] M. V. Rybin, K. L. Koshelev, Z. F. Sadrieva, K. B. Samusev, A. A. Bogdanov, M. F. Limonov, and Y. S. Kivshar, Phys. Rev. Lett. **119**, 243901 (2017).
[17] W. Chen, Y. Chen, and W. Liu, Laser Photonics Rev. **13**, 1900067 (2019).
[18] J. Wiersig, Phys. Rev. Lett. **97**, 253901 (2006).
[19] B. Wu, B. Wu, J. Xu, J. Xiao, and Y. Chen, Opt. Express **24**, 16566 (2016).
[20] Y. J. Zhang, H. Kwon, M.-A. Miri, E. Kallos, H. Cano-Garcia, M. S. Tong, and A. Alu, Phys. Rev. Applied **11**, 044049 (2019).
[21] W. Chen, Z. Xiong, J. Xu, and Y. Chen, Phys. Rev. B **99**, 195307 (2019).
[22] S. Droulias and L. Bougas, Nano Lett. **20**, 5960 (2020).
[23] S. Droulias, Phys. Rev. B **102**, 075119 (2020).
[24] L. D. Barron, *Molecular Light Scattering and Optical Activity* (Cambridge University Press, Cambridge, England, 2004).
[25] E. N. Bulgakov and A. F. Sadreev, Phys. Rev. B **78**, 075105 (2008).
[26] D. C. Marinica, A. G. Borisov, and S. V. Shabanov, Phys. Rev. Lett. **100**, 183902 (2008).
[27] Y. Plotnik, O. Peleg, F. Dreisow, M. Heinrich, S. Nolte, A. Szameit, and M. Segev, Phys. Rev. Lett. **107**, 183901 (2011).
[28] C. W. Hsu, B. Zhen, J. Lee, S.-L. Chua, S. G. Johnson, J. D. Joannopoulos, and M. Soljačić, Nature (London) **499**, 188 (2013).
[29] M. Inoue, K. Ohtaka, and S. Yanagawa, Phys. Rev. B **25**, 689 (1982).
[30] K. Sakoda, Phys. Rev. B **52**, 8992 (1995).
[31] P. Paddon and J. F. Young, Phys. Rev. B **61**, 2090 (2000).
[32] A. R. Cowan, P. Paddon, V. Pacradouni, and J. F. Young, J. Opt. Soc. Am. A **18**, 1160 (2001).
[33] S. Fan and J. D. Joannopoulos, Phys. Rev. B **65**, 235112 (2002).
[34] See Supplemental Material at http://link.aps.org/supplemental/10.1103/PhysRevLett.128.146102 for (i) the physical meaning of the p_{ij} and k_{ij} in the Hamiltonian model, (ii) three assumptions for simplifying the chiral-involved Hamiltonian, (iii) k_{12} and k_{21} reach maximum when the two resonant states satisfy the electromagnetic duality, (iv) eigenpolarization maps of TE_4 and TM_1 quasi-BICs, (v) symmetry analysis for TE4 and TM1 BIC, (vi) modeling of the chiral solution, (vii) coupling between other combinations of quasi-BICs, (viii) tuning the degeneracy of TE_4 and TM_1 quasi-BICs, (ix) the dependence of the Q factors of quasi-BICs on the perturbation Δ, (x) the coupling system when the sign of κ is flipped, and (xi) proof of $(-k_{12}k_{21}\omega_1\omega_2/p_{11}p_{22})$ being a positive real number, which includes Refs. [35–37].
[35] P. Lalanne, W. Yan, K. Vynck, C. Sauvan, and J. P. Hugonin, Laser Photonics Rev. **12**, 1700113 (2018).
[36] A. O. Govorov and Z. Fan, ChemPhysChem **13**, 2551 (2012).
[37] N. A. Abdulrahman, Z. Fan, T. Tonooka, S. M. Kelly, N. Gadegaard, E. Hendry, A. O. Govorov, and M. Kadodwala, Nano Lett. **12**, 977 (2012).
[38] W.-P. Huang, J. Opt. Soc. Am. A **11**, 963 (1994).
[39] V. Sokolov and V. Zelevinsky, Ann. Phys. (N.Y.) **216**, 323 (1992).
[40] A. O. Govorov and Z. Fan, ChemPhysChem **13**, 2551 (2012).
[41] H. Friedrich and D. Wintgen, Phys. Rev. A **32**, 3231 (1985).
[42] F. Yang, Y.-C. Liu, and L. You, Phys. Rev. A **96**, 053845 (2017).
[43] Y. Choi, C. Hahn, J. W. Yoon, and S. H. Song, Nat. Commun. **9**, 1 (2018).

[44] S. Both, H. Giessen, and T. Weiss, in *Proceedings of the CLEO: QELS_Fundamental Science* (Optical Society of America, Washington, DC, 2021), p. FTh1K. 2.
[45] A. Overvig, N. Yu, and A. Alù, Phys. Rev. Lett. **126**, 073001 (2021).
[46] M. V. Gorkunov, A. A. Antonov, and Y. S. Kivshar, Phys. Rev. Lett. **125**, 093903 (2020).
[47] J. Dixon, M. Lawrence, D. R. Barton, and J. Dionne, Phys. Rev. Lett. **126**, 123201 (2021).
[48] J. Hu, M. Lawrence, and J. A. Dionne, ACS Photonics **7**, 36 (2020).
[49] E. Mohammadi, A. Tavakoli, P. Dehkhoda, Y. Jahani, K. L. Tsakmakidis, A. Tittl, and H. Altug, ACS Photonics **6**, 1939 (2019).
[50] F. Graf, J. Feis, X. Garcia-Santiago, M. Wegener, C. Rockstuhl, and I. Fernandez-Corbaton, ACS Photonics **6**, 482 (2019).
[51] J. Feis, D. Beutel, J. Kopfler, X. Garcia-Santiago, C. Rockstuhl, M. Wegener, and I. Fernandez-Corbaton, Phys. Rev. Lett. **124**, 033201 (2020).
[52] Y. Chen, C. Zhao, Y. Zhang, and C.-W. Qiu, Nano Lett. **20**, 8696 (2020).
[53] Y. Chen *et al.*, Nat. Rev. Phys. **4**, 113 (2022).